Supplemental Document: Taking the stress out optical strain estimation: a simple and accurate method for quantifying deformation, disruption, and development in biological tissues

John J. Boyle[*†]
Maiko Kume[†]
Matthew A. Wyczalkowski[†]
Larry A. Taber[†]
Robert B. Pless[‡]
Younan Xia[§]
Guy M. Genin[¶]
Stavros Thomopoulos[*†‡]

[*]Department of Orthopaedic Surgery, Washington University, St Louis, MO 63110
[†]Department of Biomedical Engineering, Washington University, St Louis, MO 63130
[‡]Department of Computer Science and Engineering, Washington University, St Louis, MO 63130
[§]The Wallace H. Coulter Department of Biomedical Engineering, School of Chemistry and Biochemistry, Georgia Institute of Technology, Atlanta, GA 30332
[¶]Department of Mechanical Engineering & Materials Science, Washington University, St Louis, MO 63130

1 Derivation of DDE and SIMPLE algorithms

Mechanical characterization of inhomogeneous and/or geometrically complex biological tissues requires precise and accurate determination of strain fields. Digital image correlation is a well-established technique for determining strain fields on the surfaces of deforming materials[1]. The technique involves matching patterns between pairs of images to estimate the displacement of certain regions or features on a sample[1, 2]. A central limitation of estimating strain fields using existing digital image correlation methods is the need to take numerical derivatives after estimating displacements. Additionally, errors arise from sample rotation, image noise, local strain discontinuities, and large deformation. The novel warping technique proposed in this paper reduces both error and computational cost compared to existing image correlation approaches. Traditionally, strain calculations are performed after digital image correlation by binding the midpoints of matched regions to form quadrilateral elements. Then, the initial and displaced positions of the points are used to estimate the deformation gradient tensor, $\mathbf{F}$, that relates a material vector $d\mathbf{X}$ in the undeformed reference configuration to the corresponding spatial vector $d\mathbf{x}$ in the deformed configuration using a least squares fit (LSF)[1]:

$$d\mathbf{x} = \mathbf{F}d\mathbf{X} \tag{1.1}$$

The Green-Lagrange strain tensor, $\mathbf{E}$, can then be then calculated as:

$$\mathbf{E} = 0.5(\mathbf{F}^T\mathbf{F} - \mathbf{I}) \tag{1.2}$$

where $\mathbf{I}$ is the second order identity tensor. These methods are all based on displacement fields.

Both rigid and non-rigid methods exist to register undeformed to deformed regions of an image and thereby estimate displacement fields (Figure 1). Rigid registration uses standard cross correlation of undeformed and deformed regions to estimate the displacements of the midpoints. $\mathbf{F}$ is calculated from an LSF of the displacements. Non-rigid approaches involve optimization to minimize an energy function iteratively:

$$\sum_x [I(\mathbf{W}(\mathbf{x};\mathbf{p})) - T(\mathbf{x})]^2 \tag{1.3}$$

where $T(x)$ is a template image, and $I(\mathbf{W}(\mathbf{x};\mathbf{p}))$ is an image, I, warped by a defined warping function $\mathbf{W}(\mathbf{x};\mathbf{p})$ whose warping parameter $\mathbf{p}$ can be modulated. The Lucas-Kanade (LK) inverse compositional algorithm[3] iterates using the following increments for $\mathbf{p}$:

$$\Delta\mathbf{p} = H^{-1}\sum_x \left[\nabla I\frac{\partial\mathbf{W}}{\partial\mathbf{p}}\right]^T [T(\mathbf{x}) - I(\mathbf{W}(\mathbf{x};\mathbf{p}))] \tag{1.4}$$

until the norm $\|\Delta p\|$ drops below a defined threshold, where H is the Gauss-Newton approximation to the Hessian matrix:

$$H = \left[\nabla I\frac{\partial\mathbf{W}}{\partial\mathbf{p}}\right]^T \left[\nabla I\frac{\partial\mathbf{W}}{\partial\mathbf{p}}\right] \tag{1.5}$$

We refer to this method as the LK method, where strains are calculated from Eq. (1.1) performed on a least squares fit to estimates of the displacement field. We present here a novel technique to circumvent the LSF deformation gradient tensor calculation based on the midpoints in Eq. (1.1). The new method allows the intrinsic calculation of $\mathbf{F}$ during digital image correlation by carefully choosing the warping function during the LK correlation. By removing the calculation in Eq. (1.1), this new method is more precise,

less susceptible to noise, and more computationally efficient (Figure 3). For the specific comparison cases presented here, the warping function $\mathbf{W}(\mathbf{x};\mathbf{p})$ in Eq. 1.3, is chosen to be a first order an affine warp with a linear translation:

$$\mathbf{W}(\mathbf{x};\mathbf{p}) = \begin{bmatrix} 1+p_1 & p_3 & p_5 \\ p_2 & 1+p_4 & p_6 \\ 0 & 0 & 1 \end{bmatrix} \begin{bmatrix} x \\ y \\ 1 \end{bmatrix} \tag{1.6}$$

where p_5 and p_6 are the translations in the x and y coordinates, respectively. Other techniques have demonstrated that displacement tracking can be improved by incorporating a higher order warping function[4]. However, we deliberately choose our warp to be of the first order. By restricting the warp to be of the first order, we mimic the definition of the deformation gradient tensor. The deformation gradient tensor considers only the deformation of an infinitesimal neighborhood about a point and thereby assumes the deformation can be approximated by a linear, first order, transformation. This is similar to Taylor's Theorem in elementary calculus, which states that the approximation $dy = f'(x)dx$ can be made if dx and dy are infinitesimally small[5]. Therefore, by choosing a first order warp, the deformation gradient tensor has a one to one correspondence with our chosen warping function. The deformation gradient tensor can be then directly extracted from the first four components of the warp:

$$\mathbf{F} = \begin{bmatrix} 1+p_1 & p_3 \\ p_2 & 1+p_4 \end{bmatrix} \tag{1.7}$$

thereby circumventing any least squares fit of the displacement field required in all prior methods (DDE method, Fig. 1).

The SIMPLE method for determining strain field inhomogeneity and strain concentrations was then developed by considering the difference between the DDE and LK solutions. Both the DDE and LK methods assume deformation is linear and homogeneous: they both compute a linear finite deformation gradient tensor. However, DDE calculates the deformation of a single region, while LK calculates the deformation between several regions. Therefore, any difference between the LK and DDE solutions represents a high-order, non-linear deformation and provides a robust detection criteria for inhomogeneity within a strain field. Furthermore, if the difference between the LK and DDE solutions is locally high, the strain field must be locally inhomogeneous and a locally inhomogeneous strain field indicates the emergence of a strain concentration. To calculate SIMPLE, a elementary difference approach is employed (Fig 3. A, B):

$$\mathbf{\Delta} = \mathbf{E}_{DDE} - \mathbf{E}_{LK} \tag{1.8}$$

This method is analogous to a spatial high pass filter of the strain field. To construct the high pass filter, consider subtracting the calculated strain for a particular correlated element from the average strain calculated over some small region Ω:

$$\frac{1}{\Omega}\int_{\Omega} \epsilon_{xx} d\Omega - \epsilon_{xx} = \delta xx \tag{1.9}$$

where δ_{xx} is the strain concentration in the xx direction and ϵ_{xx} is the strain in the xx direction. We can then define the average strain over the region Ω as ϵ^*_{xx}:

$$\frac{1}{\Omega}\int_{\Omega} \epsilon_{xx} d\Omega = \epsilon^*_{xx} \tag{1.10}$$

Then by assuming small strain:

$$\lambda_{xx} = \epsilon_{xx} + 1 \tag{1.11}$$

$$\lambda^*_{xx} = \epsilon^*_{xx} + 1 \tag{1.12}$$

Combining Eq. 1.9-1.12:

$$\lambda^*_{xx} - \lambda_{xx} = \delta xx \tag{1.13}$$

Which is analogous to the tensor equation:

$$\mathbf{F}^* - \mathbf{F} = \mathbf{\Delta} \tag{1.14}$$

Where $\mathbf{F}^*$ is $\mathbf{F}_{DDE}$ and $\mathbf{F}$ is $\mathbf{F}_{LK}$ and Δ is a strain concentration matrix.

2 A note on the compatibility of strain fields averaged over finite regions

The DDE method is more accurate than the Lucas Kanade displacement-based or standard cross-correlation methods for estimating average strains over discrete regions of finite size. This accuracy is attained by estimating deformation gradient tensors without first calculating displacement fields of the centroids of these regions. We emphasize here that displacement fields can be calculated uniquely from DDE estimates of strain fields only in special cases, and that if a displacement field is required the Lucas Kanade displacement-based approach is a better choice.

The reason for this relates to the problem of "strain compatibility" that is well known in mechanics: unique components of a displacement field can be determined from the more numerous components of a strain field only if the spatial variations of these strain fields satisfy certain conditions. For example, for linearized strains in two dimensions, the components of the strain tensor $\epsilon(x, y)$ in a Cartesian (x, y) coordinate frame must satisfy (e.g., [6]):

$$\frac{\partial^2 \epsilon_{xx}(x,y)}{\partial y^2} - 2\frac{\partial^2 \epsilon_{xy}(x,y)}{\partial x \partial y} + \frac{\partial^2 \epsilon_{yy}(x,y)}{\partial x^2} = 0. \tag{2.1}$$

However, rather than reporting a continuous strain field $\epsilon_{\alpha\beta}(x, y)$ that must satisfy the compatibility relations, the DDE method reports components of strain $\bar{\epsilon}^{(i)(j)}_{\alpha\beta}$ averaged over a region of dimensions $L \times L$ at each position $\{i, j\}$, usually on a regular grid (e.g., Figure S1):

$$\bar{\epsilon}^{(i)(j)}_{\alpha\beta} = \frac{1}{L^2} \int_{(i-1)L}^{iL} \int_{(j-1)L}^{jL} \epsilon_{\alpha\beta}(x, y) dx dy \tag{2.2}$$

As shown below, a compatible strain field averaged over an array of finite, discrete regions, does not in general satisfy the compatibility relations. On the one hand, this means that finding a unique displacement field that satisfies a DDE-estimated strain field is usually not possible. On the other, this means that DDE is never constrained by specific models or interpolations of strain fields.

The reason for this relates to computation of the second derivatives in Equation 2.1: the finite difference approximation to $\frac{\partial^2 \bar{\epsilon}^{(i)(j)}_{yy}}{\partial x^2}$ equals the continuous value of $\frac{\partial^2 \epsilon_{yy}}{\partial x^2}(x_0, y_0)$ at the center (x_0, y_0) of region (i, j) only under special conditions. The finite difference approximation of this term for the DDE-estimated average strain fields is:

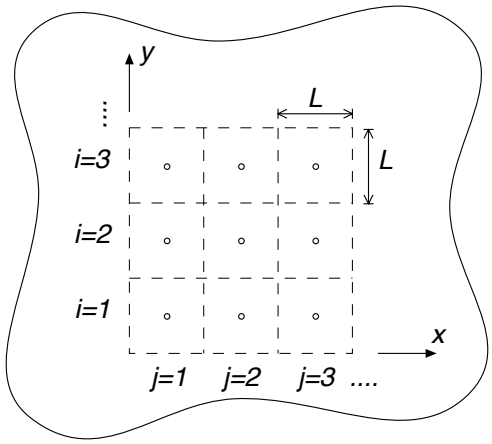

Figure S1: The DDE method is often implemented on a regular grid within a strained body.

$$\frac{\partial^2 \bar{\epsilon}_{yy}^{(i)(j)}}{\partial x^2} = \frac{\bar{\epsilon}_{yy}^{(i)(j+1)} - 2\bar{\epsilon}_{yy}^{(i)(j)} + \bar{\epsilon}_{yy}^{(i)(j-1)}}{L^2} \tag{2.3}$$

and, for $x_0 = L(j + \frac{1}{2})$ and $y_0 = L(i + \frac{1}{2})$, and L sufficiently small, the finite difference approximation is:

$$\frac{\partial^2 \epsilon_{yy}}{\partial x^2}(x_0, y_0) \approx \frac{\epsilon_{yy}(x_0 + L, y_0) - 2\epsilon_{yy}(x_0, y_0) + \epsilon_{yy}(x_0 - L, y_0)}{L^2} \tag{2.4}$$

The approximation in Equation 2.4 will, for a sufficiently smooth function, equal the exact second derivative in the limit of L approaching zero. The approximation in Equation 2.3 to approach this same value for all choices of x_0 and y_0 (i and j) if the average value of $\epsilon_{yy}(x, y)$ in a region happens to equal the value at the center of the region (that is, $\bar{\epsilon}_{yy}^{(i)(j)} = \epsilon_{yy}(x_0, y_0)$), or if the difference between the two varies in specific ways, such as:

$$\bar{\epsilon}_{yy}^{(i)(j)} = \epsilon_{yy}(x_0, y_0) + f_1(y_0) + x_0 f_2(y_0) + C_1 \tag{2.5}$$

where C_1 is an arbitrary constant and f_1 and f_2 are functions of y_0 only. Similar relations can be derived for the other terms in Equation 2.1. The consequence is that, no matter how fine the discretization, discrete derivatives of DDE-estimated strain fields should never be forced to meet the compatibility equations.

As a simple example, consider the following strain field that satisfies Equation 2.1:

$$\epsilon_{\alpha\beta} = \begin{bmatrix} 0 & 2Ax^3y \\ 2Ax^3y & Ax^4 \end{bmatrix} \tag{2.6}$$

In the absence of any experimental or measurement error, the averaged strains that the DDE algorithm should report are the following:

$$
\begin{aligned}
\bar{\epsilon}_{xy}^{(i)(j)} &= \frac{1}{L^2}\int_{(i-1)L}^{iL}\int_{(j-1)L}^{jL} 2Ax^3 y dxdy \\
&= 2AL^4\left((j-\frac{1}{2})^3+\frac{1}{4}(j-\frac{1}{2})\right)(i-\frac{1}{2}) \\
\bar{\epsilon}_{xx}^{(i)(j)} &= 0 \qquad (2.7)\\
\bar{\epsilon}_{yy}^{(i)(j)} &= \frac{1}{L^2}\int_{(i-1)L}^{iL}\int_{(j-1)L}^{jL} Ax^4 dxdy \\
&= AL^4\left((j-\frac{1}{2})^4+\frac{1}{2}(j-\frac{1}{2})^2+\frac{1}{80})\right) \qquad (2.8)
\end{aligned}
$$

Note that these can be written in terms of x_0 and y_0 as:

$$
\begin{aligned}
\bar{\epsilon}_{xy}^{(i)(j)} &= 2A\left(x_0^3+\frac{x_0L^2}{4}\right)y_0 = \epsilon_{xy}(x_0,y_0)+2Ax_0y_0\left(\frac{L}{2}\right)^2 \\
\bar{\epsilon}_{yy}^{(i)(j)} &= Ax_0^4+AL^2\left(\frac{x_0^2}{2}+\frac{L^2}{80}\right) = \epsilon_{yy}(x_0,y_0)+AL^2\left(\frac{x_0^2}{2}+\frac{L^2}{80}\right) \qquad (2.9)
\end{aligned}
$$

Finite difference approximations to the derivatives in the compatibility equation are:

$$
\begin{aligned}
\frac{\partial^2\bar{\epsilon}_{xy}^{(i)(j)}}{\partial x\partial y} &\approx \frac{1}{4L^2}\left(\bar{\epsilon}_{xy}^{(i+1)(j+1)}+\bar{\epsilon}_{xy}^{(i-1)(j-1)}-\bar{\epsilon}_{xy}^{(i-1)(j+1)}+\bar{\epsilon}_{xy}^{(i+1)(j-1)}\right) \\
&= 6AL^2(j^2-j+\frac{2}{3}) = 6Ax_0^2+\frac{5}{2}AL^2 \qquad (2.10)\\
\frac{\partial^2\bar{\epsilon}_{yy}^{(i)(j)}}{\partial x^2} &= \frac{\bar{\epsilon}_{yy}^{(i)(j+1)}-2\bar{\epsilon}_{yy}^{(i)(j)}+\bar{\epsilon}_{yy}^{(i)(j-1)}}{L^2} \\
&= 12AL^2(j^2-j+\frac{1}{2}) = 12Ax_0^2+3AL^2 \qquad (2.11)
\end{aligned}
$$

Substituting into the compatibility relation Equation 2.1 yields:

$$
\begin{aligned}
\frac{\partial^2\epsilon_{xx}(x,y)}{\partial y^2}-2\frac{\partial^2\epsilon_{xy}(x,y)}{\partial x\partial y}+\frac{\partial^2\epsilon_{yy}(x,y)}{\partial x^2} &= -2\left(6Ax_0^2+\frac{5}{2}AL^2\right)+12Ax_0^2+3AL^2 \\
&= -2AL^2 \\
&\neq 0 \qquad (2.12)
\end{aligned}
$$

In this example, and in general, forcing strain compatibility into the direct estimation of strain fields would be incorrect.

From the above example it is clear that forcing strain compatibility is not always appropriate and may result in the incorrect calculations of strains. Strain compatibility was originally introduced into digital image correlation to ensure that strain fields were continuous and that minor mis-tracking would not introduce errors into the strain field [6]. With the improved accuracy and precision of DDE coupled with the direct

calculation of strain by neglecting displacements, strain compatibility can be relaxed, allowing incompatible, non-continuous, strain fields. Detecting when strain fields become incompatible is the motivation for the derivation of the SIMPLE method. The SIMPLE method, in essence, looks at the difference between strain fields in which compatibility is not enforced (DDE) and strain fields in which compatibility is enforced (LK). By comparing the two, the SIMPLE method is able to detect precisely when and where strain fields become incompatible and non-smooth. In the example considered above, SIMPLE would calculate the non-zero difference between the two results (Eq.2.12).

3 Experimental methods

3.1 Fabrication and testing of PDMS scaffolds with gradients in stiffness

PDMS sheets (N=3) with gradients in stiffness were fabricated according to published methods[7]. Briefly, Sylgard 184 PDMS was mixed at two base:curing agent ratios: 10:1 and 20:1. Silanized glass slides and a Teflon spacer were used to create a mold. The two PDMS mixtures were then poured into the mold such that the 10:1 mixture was on the bottom and the 20:1 mixture was on the top. Filled molds were placed on top of a hot plate at 120 C for 90 min so that a temperature gradient developed vertically along the mold, creating a gradient in cross linker activation and a subsequent gradient in stiffness. Polymerized PDMS scaffolds were rinsed in hexane to swell the scaffold and remove residual crosslinkers, preventing further polymerization. Scaffolds were then sprayed lightly with black latex spray paint to produce a random surface speckle texture, and placed in a custom designed cyclic tensile machine. Scaffolds were pulled in tension to 10% grip-to-grip strain at a rate of 0.1 Hz. Videos of the test were captured using an Illunis VMV-8M camera for subsequent strain analysis.

3.2 Fabrication and testing of collagen scaffolds with gradients in stiffness

Collagen scaffolds with gradients in stiffness were created using reconstituted collagen and simulated body fluid-induced mineralization according to a published procedures (N=4)[8]. Briefly, lyophilized collagen (Elastin Products Company, product no. C857) was dissolved in a dilute solution of hydrochloric acid, homogenized, degassed, and pumped into cylindrical casts (4 mm). Collagen casts were polymerized in TES buffer (135 mM Ntris(hydroxymethyl)-methyl-2-aminoethane sulfonic acid, 30 mM NaCl, and 30 mM Na2PO4 in distilled water; pH 7.5) at 37 C for 1 hr and then allowed to soak at room temperature overnight in de-ionized water [8]. Following soaking, collagen scaffolds were dehydrated in 95% ethanol and then allowed to air dry overnight. Scaffolds were placed in 10X simulated body fluid solution with 5 mg/ml fetuin at a pH of 7.4 for mineralization[8]. Scaffolds were slowly drawn out of the solution to create a gradient in mineralization[9]. Following mineralization, scaffolds were dehydrated a second time in 95% ethanol and allowed to air dry overnight. Scaffolds were then sprayed lightly with Verhoffs stain to produce a random surface speckle texture. For mechanical testing, scaffolds were loaded in tension in a PBS bath (37°C) at a strain rate of 0.1 %/s using a materials testing frame (Instron Electropuls E1000). Videos of the test were captured using an Illunis VMV-8M camera for subsequent strain analysis.

3.3 Fabrication and testing of vinylidene chloride sheets

Commercially available vinylidene chloride sheets (Saran Premium Wrap, SC Johnson) were coated in white latex paint and allowed to dry overnight (N=2). After drying, the sheets were cut into 20 x 5 mm^2 sheets and sprayed lightly with black latex spray paint to produce a random surface speckle texture. Sheets were

gripped using spring clamps and loaded in tension at a strain rate of 0.1 %/s using a materials testing frame (Instron Electropuls E1000). Videos of the test were captured using an Illunis VMV-8M camera for analysis.

3.4 Embryonic injury models

Videos for elliptical incision and circular punched embryonic injury models were obtained from a previously described experiment[10]. All wounds were made at early embryonic time points where cells do not reside on a substrate (Hamburger-Hamilton 5-6). Linear ablated wounds were created using the Gastromaster microsurgery device (Xenotek Engineering) with white tips, which lyses cells with no direct mechanical contact[11].

4 Collagen scaffold results

DDE accurately detected a gradient in strain between the top and the bottom of the scaffold, demonstrating a mineral-induced gradient in stiffness along the length of the scaffold (Supplemental Figure 1A,B, Supplemental Video 2). In contrast, XCOR demonstrated unrealistically high strains, likely due to errors resulting from slight rotation of the sample during testing (Supplemental Figure 1C,D). These errors were exacerbated at high grip-to-grip strains with the XCOR technique (Supplemental Figure 1G,H), whereas DDE tracked a local strains as high as 0.18 (Supplemental Figure 1E,F).

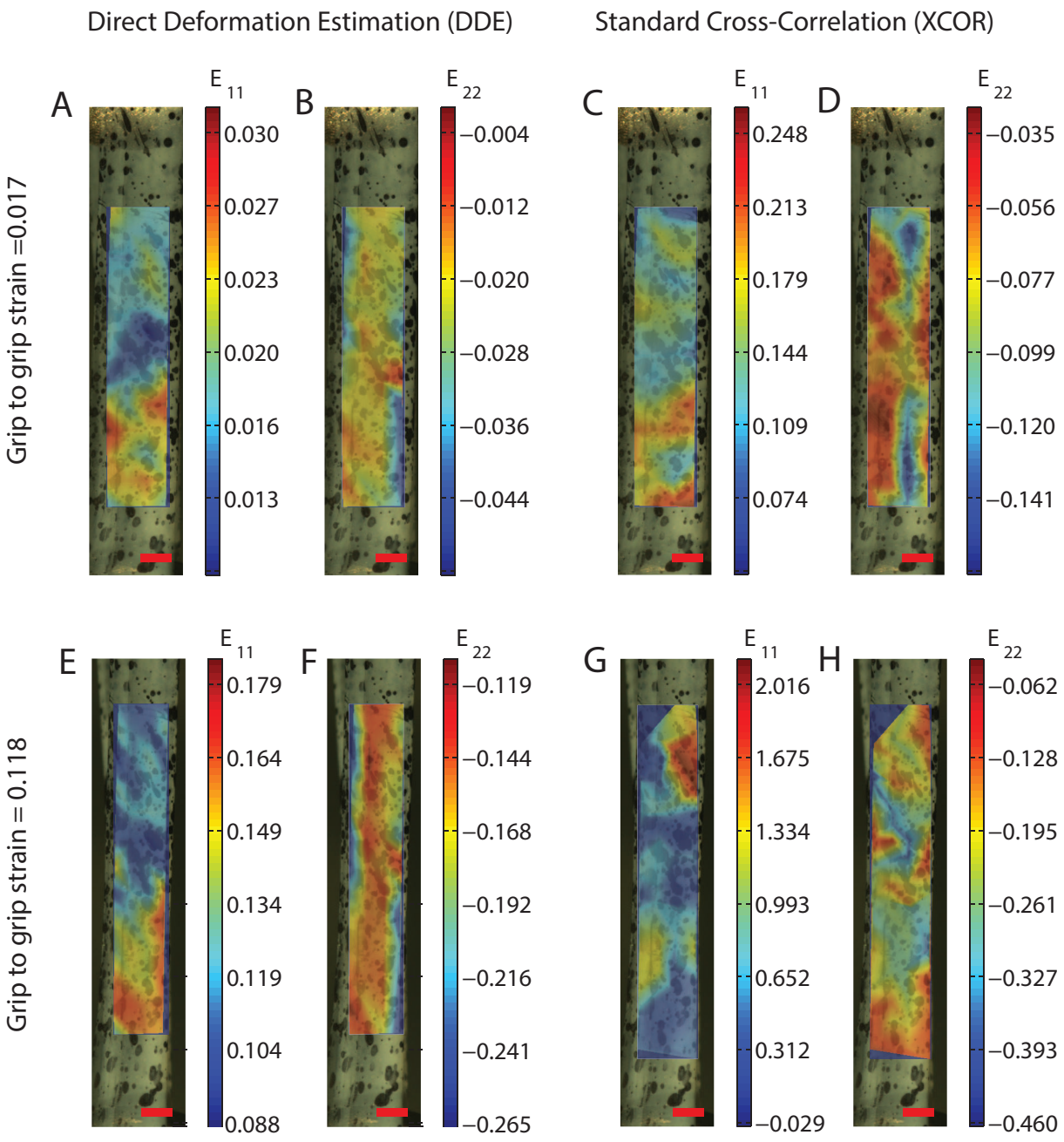

Figure S2: Small and large grip-to-grip strains of collagen scaffolds with spatial gradients in mineral content, tested in tension. **(A, B, E, F)** DDE revealed a gradient in material strain for low and high grip-to-grip strains. **(C, D)** At low grip-to-grip strains, XCOR revealed similar trends to DDE. However, the values of strains measured were unrealistically high and are likely due to noise. **(G, H)** At high grip-to-grip strains, XCOR reported strains over 2. This was clearly erroneous based on visual inspection of the specimen, demonstrating the limitations of the XCOR technique for large strains in inhomogeneous samples.

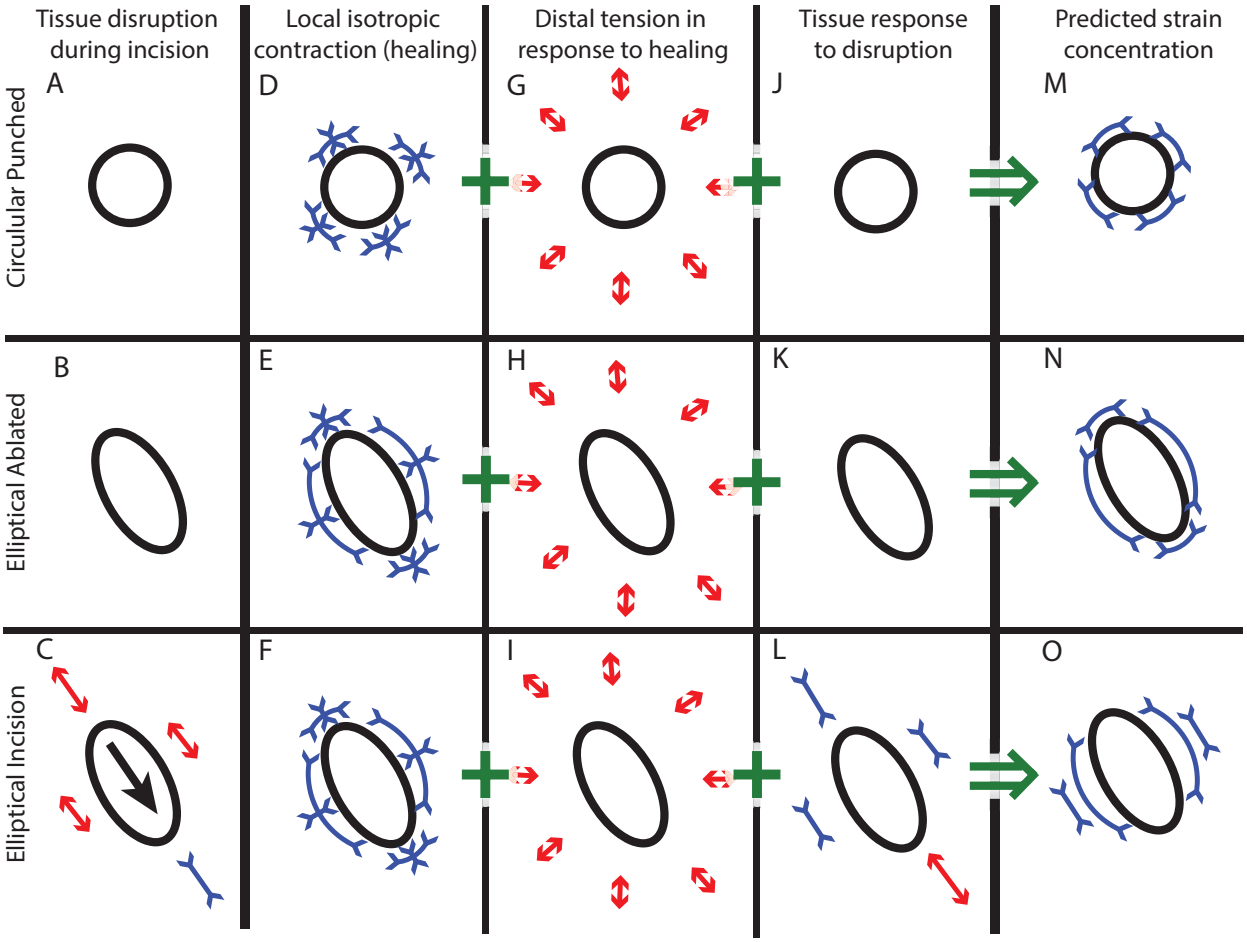

Figure S3: Embryonic wounds were created using three methods: circular wounds created with a punch (top row), elliptical wounds created by ablation (middle row), and elliptical wounds created by incision with a micro-scalpel (bottom row). Strains were analyzed to delineate how three mechanisms combine to change the wound: **(D,E,F)** localized isotropic contraction around the wound, **(G,H,I)** passive elastic recovery of tissue distal to the wound, and **(J,K,L)** stretching introduced during wound creation. **(A, B, C)** Injuries induced by circular punching and elliptical ablation do not introduce additional deformations into the wound healing system. However, the elliptical incision method adds tension in the wake of the blade and compression ahead of the blade. **(A, B, C)** Localized isotropic contraction of wounds is expected at the border of the wound for all wound scenarios. **(E, E, F)** In response to localized isotropic contraction near the wound, regions distal to the wound are expected to be in tension, as cells near the wound pull inward to close the injury. **(J, L, K)** Since no additional deformations were introduced during wounding for circular punched and elliptical ablated injuries, no response to the wounding is expected in these cases. For elliptical incision injuries, however, the tissue is expected to respond to the incision deformations **(C)** by returning to its original state. **(M, N, O)** Strain concentrations are expected to arise at the wound border due to the localized isotropic contraction in all wound scenarios. For elliptical incision injuries, however, strains introduced during wounding combined with the localized isotropic contraction should result in strain concentrations primarily along the flanks of the elliptical wound.

5 Supplemental video legends

Supplemental Video 1: PDMS sheets with spatial gradients in stiffness were cyclically stretched. DDE was able to detect smooth gradients in local strain at low and high grip-to-grip strains. In contrast, XCOR failed to detect gradients at low grip-to-grip strains and detected irregular gradients in local strain at high grip-to-grip strains.

Supplemental Video 2: Tensile tests-to-failure of collagen scaffolds with gradients in mineral content were performed. DDE revealed gradients of strain along the length of the scaffolds throughout the test whereas XCOR failed to accurately determine local strain patterns.

Supplemental Video 3: Vinylidene chloride sheets were tested in tension to failure. The SIMPLE method accurately detected strain concentrations predictive of crack initiation formation and was able to track crack propagation. XCOR only tracked the strain concentration for limited time, missing the initiation of the strain localization and failing to track the crack after it formed.

Supplemental Videos 4, 5, and 6: Embryonic wounds were created using three methods: circular wounds created with a punch (Supplemental Video 4), elliptical wounds created by ablation (Supplemental Video 5), and elliptical wounds created by cutting with a micro-scalpel (Supplemental Video 6). The DDE and SIMPLE algorithms described the spatial and temporal patterns of embryonic wound closure, while the XCOR algorithm revealed only noise.

References

[1] Hubert W. Schreier, Michael Albert Sutton, and Jean-Jose Orteu. Image Correlation for Shape, Motion and Deformation Measurements. Springer, 2009.

[2] HA Bruck, SR McNeill, MA Sutton, and WH Peters Iii. Digital image correlation using Newton-Raphson method of partial differential correction. Experimental Mechanics, pages 261–267, 1989.

[3] Simon Baker and Iain Matthews. Lucas-Kanade 20 Years On: A Unifying Framework. International Journal of Computer Vision, 56(3):221–255, February 2004.

[4] Kai Y Lim, Jonathan T Henderson, and Corey P Neu. Cell and tissue deformation measurements: texture correlation with third-order approximation of displacement gradients. Journal of biomechanics, 46(14):2490–6, September 2013.

[5] Lawrence E. Malvern. Introduction to the mechanics of a continuous medium. Prentice-Hall, 1969.

[6] William S Slaughter. The linearized theory of elasticity. Springer, 2002.

[7] Peng-Yuan Wang, Wei-Bor Tsai, and Nicolas H Voelcker. Screening of rat mesenchymal stem cell behaviour on polydimethylsiloxane stiffness gradients. Acta biomaterialia, 8(2):519–30, February 2012.

[8] LJ Smith, J Boyle, Z Li, JD Pasteris, G Genin, and S Thomopoulos. Bulk Mineralization Stiffens Collagen Scaffolds. In Orthopaedic Research Society, volume 97, 2012.

[9] Xiaoran Li, Jingwei Xie, Justin Lipner, Xiaoyan Yuan, Stavros Thomopoulos, and Younan Xia. Nanofiber scaffolds with gradations in mineral content for mimicking the tendon-to-bone insertion site. Nano letters, 9(7):2763–8, July 2009.

[10] MA Wyczalkowski, VD Varner, and LA Taber. Computational and Experimental Study of the Mechanics of Embryonic Wound Healing. Journal of the Mechanical Behavior of Biomedical Materials, 28:125–146, 2013.

[11] Victor D Varner and Larry a Taber. Not just inductive: a crucial mechanical role for the endoderm during heart tube assembly. Development, 139(9):1680–90, May 2012.